J. Min. Metall. Sect. B-Metall. 62 (2) (2026) 195 - 209

Journal of Mining and Metallurgy,
Section B: Metallurgy

ROLE OF MOLYBDENUM IN MINING GRADE Ni-Cr-Mo STEELS FROM AN INDUSTRIAL PERSPECTIVE

Varun Kumar Kurapati [a], Makkuva Kalyan Phani [a, *], Arghya Majumder [b]

[a] Department of Metallurgical Engineering, O.P. Jindal University, Raigarh, Chhattisgarh, India
[b] School of Mines and Metallurgy, Kazi Nazrul University, Asansol, West Bengal, India

(Received 24 October 2025; Accepted 23 June 2026)

Abstract

Nickel-chromium-molybdenum (Ni-Cr-Mo) steels are widely used in critical engineering applications that require high strength, wear resistance, and fatigue performance. In the present study, the influence of molybdenum content on the microstructural evolution and mechanical properties of carburized EN36C and AISI 9315 steels was investigated. The steels were subjected to gas carburizing at 920 °C in a sealed quench furnace, followed by quenching and tempering. Detailed characterization was performed using microstructural analysis, hardness measurements, case depth evaluation, tensile testing, impact testing, and fractography. The results revealed significant differences in microstructure and mechanical performance between the two steel grades. AISI 9315 steel, with relatively higher molybdenum content, exhibited improved hardenability, higher hardness, enhanced case characteristics, and superior mechanical properties compared to EN36C steel. Variations in retained austenite content and fracture behavior were also observed as a function of molybdenum content and heat treatment response. The study demonstrates the significant role of molybdenum in controlling phase transformation behavior and enhancing the overall performance of carburized Ni-Cr-Mo steels.

Keywords: *Ni-Cr-Mo steels; Gas carburizing; Case depth; Microhardness; Fractography*

1. Introduction

Nickel-Chromium-Molybdenum (Ni-Cr-Mo) alloy steels are extensively used in critical engineering applications such as automotive transmission systems, aerospace components, mining machinery, drilling tools, gears, shafts, and heavy-duty power transmission equipment due to their excellent combination of surface hardness, wear resistance, fatigue strength, and core toughness after carburizing and heat treatment [1–4]. Among these steels, EN36C and AISI 9315 are widely employed as case-hardening steels because of their superior hardenability and ability to develop a hard martensitic case with a comparatively tough and ductile core [5–7]. The performance of these steels is strongly dependent on carburizing parameters, alloy chemistry, quenching conditions, tempering response, and retained austenite stability developed during heat treatment [8–10].

Recent studies have demonstrated that heat treatment plays a crucial role in controlling phase transformation behavior, carbide precipitation, residual stresses, retained austenite stability, wear resistance, and fatigue performance of case-hardened steels [11–14]. In particular, alloying elements such as molybdenum significantly influence hardenability, suppression of pearlite and bainite transformation, martensitic transformation kinetics, and secondary hardening behavior during tempering [15–17]. Although several investigations have reported the general mechanical and tribological behavior of carburized steels, limited studies are available comparing the microstructural evolution and retained austenite characteristics of EN36C and AISI 9315 steels under similar gas carburizing and post-heat-treatment conditions. Furthermore, the specific influence of slight variations in molybdenum content on retained austenite formation, hardness distribution, tensile behavior, impact toughness, and fracture characteristics has not been adequately addressed.

In industrial applications such as gears, shafts, and mining components, optimization of retained austenite and case properties is critical for achieving improved fatigue resistance, dimensional stability, and service life. However, there remains a lack of systematic understanding regarding the relationship between molybdenum content, carburizing response, and resultant microstructural and mechanical properties in these two commercially important steels.

Corresponding author: kalyan.makkuva@opju.ac.in

https://doi.org/10.2298/JMMB251024015K

Therefore, a comparative investigation under identical processing conditions is necessary to establish the role of alloy chemistry in determining the final performance of carburized components.

The present study focuses on the microstructural and mechanical characterization of gas carburized EN36C and AISI 9315 steels subjected to carburizing, reheat quenching, tempering, and sub-zero treatment conditions. Special emphasis is given to understanding the influence of molybdenum content on retained austenite evolution, hardness profile, tensile strength, impact toughness, case characteristics, and fracture behavior. The study aims to provide insights into optimizing heat treatment strategies and material selection for demanding engineering applications requiring superior wear resistance and mechanical reliability.

2. Methods and Materials

Due to their significance in industrial applications such as mining drill bits, drilling machines, and automotive components, two different steel variations, Sample A (AISI 9315) and Sample B (EN36C), were carefully selected as representative samples for this investigation. The molybdenum content of Sample B is 0.25%, but Sample A has a lower molybdenum value of 0.08%. Using Electrical Discharge Machining (EDM), longitudinal specimens were methodically extracted from forging parts and precisely formed to guarantee consistency and accuracy in sample geometry and measurements.

Table 1 reveals a striking similarity in the composition of these two alloys, with the notable exception being the Molybdenum content. Figure 1 presents a comprehensive flow diagram outlining the steel evaluation process, wherein the steel samples underwent primarily gas carburizing heat treatment.

Table 1. *Chemical composition of steel variants*

Element	AISI 9315 (Sample A)	EN36C (Sample B)
C	0.16	0.15
Mn	0.55	0.5
Si	0.25	0.22
Ni	3.0	3.1
Mo	0.1	0.25
Cr	1.3	1.1
P	0.020	0.015
S	0.015	0.013

2.1. Heat Treatment

Figure 2. A standardized thermal treatment programme including gas carburizing, reheat quenching, and tempering was applied to both samples. Gas carburizing, which was carried out at about 920°C, allowed carbon to diffuse into the surface of the steel. To reduce the amount of retained austenite in the carburized layers, reheat quenching was then applied. The mechanical characteristics of the samples were further enhanced by subsequent tempering. The samples were subjected to different heat treatment methods like:

1. Hardening and Tempering (H+T)
2. Carburizing, Hardening and Tempering (C+H+T)
3. Carburizing, Hardening, Tempering and sub-zero Treatment (C+H+T+S)
4. Carburizing, Hardening, Tempering, sub-zero Treatment and Tempering (C+H+T+S+T)

The selected carburizing temperature, quenching conditions, tempering parameters, and sub-zero treatment conditions were adopted based on standard industrial operating ranges commonly employed for EN36C and AISI 9315 steels to achieve the desired case depth, hardness, and mechanical performance. The vertical axis corresponding to Carbon Potential (Cp) is expressed in percentage (%C), while the Nitrogen content is represented in flow rate/concentration units as recorded by the furnace control system during the carburizing process.

2.2. Sample Preparation and Analysis

The samples were sectioned using EDM, and thorough testing procedures were performed using an automated Universal Testing Machine (UTM) in compliance with ASTM guidelines. The chemical composition of the material was examined using a BAIRD Optical Emission Spectroscope. For the microstructural analysis, a Leica optical microscope and a Tescan Vega III SEM were used. The EMCO Tester was utilized to measure the Effective case depth at 0.5HV load for Micro Hazard measurement.

2.3. Microstructural analysis

Samples underwent grinding, polishing, and 2% Nital etching for microstructural analysis. Optical microscopy revealed a martensitic matrix with retained austenite and carbides, identified using ASTM chart comparisons for accurate phase characterization. This complex microstructural mixer

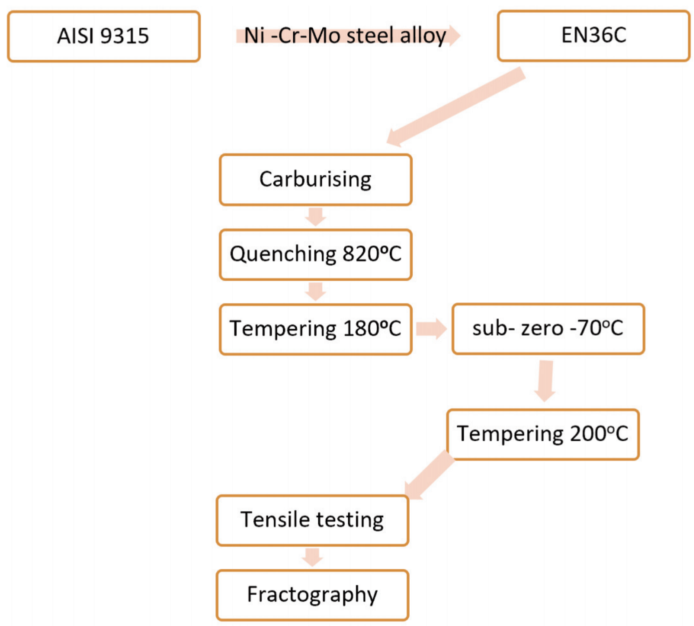

Figure 1. *Evaluation process diagram of both alloys*

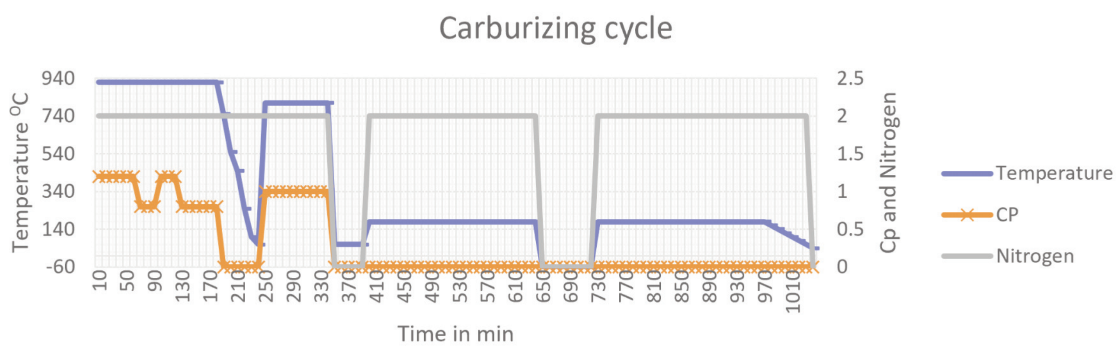

Figure 2. *Heat treatment cycle given to the two samples, Gas carburizing and followed by quenching Tempering and sub-zero treatment, Here Cp stands for Carbon potential which is given as wt % of Carbon and Nitrogen flow rate expressed as Nm^3/h*

clarifies the transformation processes that take place during heat treatment and offers significant information about the mechanical and performance qualities of the material [11].

2.4. Mechanical Testing

Tensile and hardness tests followed ASTM standards, providing crucial mechanical data. Adhering closely to specified testing procedures ensures the reliability and accuracy of the data collected, facilitating a comprehensive understanding of the material's mechanical behavior following heat treatment [12-14].

2.5. Measurement of case depth

Vickers hardness values were converted to HRC values in order to establish the effective case depth using a microhardness traverse on polished metallographic sections. Significant information about the calibre and functionality of carburized components was obtained by analysing the case depth and surface hardness.

2.6. Fractography

Fractured samples were analyzed using the SEM Tescan Vega III, revealing the impact of retained austenite and molybdenum on fracture behavior. The study elucidates fracture morphology, propagation paths, and material response, offering insights to enhance structural integrity and fracture resistance in metallurgical applications under varying processing conditions.

3. Results and Discussion

3.1. Microstructural characterization

The microstructural examination revealed a predominant martensitic phase characterized by 5 to 10% retained austenite content. Martensite, known for its exceptional hardness, forms as a result of rapid quenching from supersaturated austenite, facilitated by a shear transformation mechanism [5]. It is noteworthy that the hardness of martensite exhibits a consistent increase in correlation with higher carbon content, typically up to around 0.7 wt%. RA values are based on practical industrial metallurgical assessment and comparative interpretation rather than direct quantitative metallographic measurement.

Heating induces phase transformation, forming lower bainite and carbide, with retained austenite in a tempered martensite matrix. Retained austenite is known to wield a direct influence on mechanical properties [5], making it a crucial focus of this investigation. Furthermore, the core region of the steel displayed characteristics of low carbon tempered martensite and relatively lower levels of epsilon carbide [13-15].

Molybdenum is known to significantly enhance hardenability by delaying diffusional phase transformations such as pearlite and bainite formation during cooling. This occurs due to the reduction in carbon diffusivity and retardation of carbide precipitation, which shifts the transformation curves toward longer times, thereby promoting martensitic transformation even at relatively lower cooling rates. The addition of Mo also contributes to improved martensite stability through solid solution strengthening and by influencing carbon partitioning between martensite and retained austenite.

Further, Mo affects the martensitic transformation characteristics by lowering the martensite start (Ms) temperature, which promotes the retention of austenite after quenching. The stability of retained

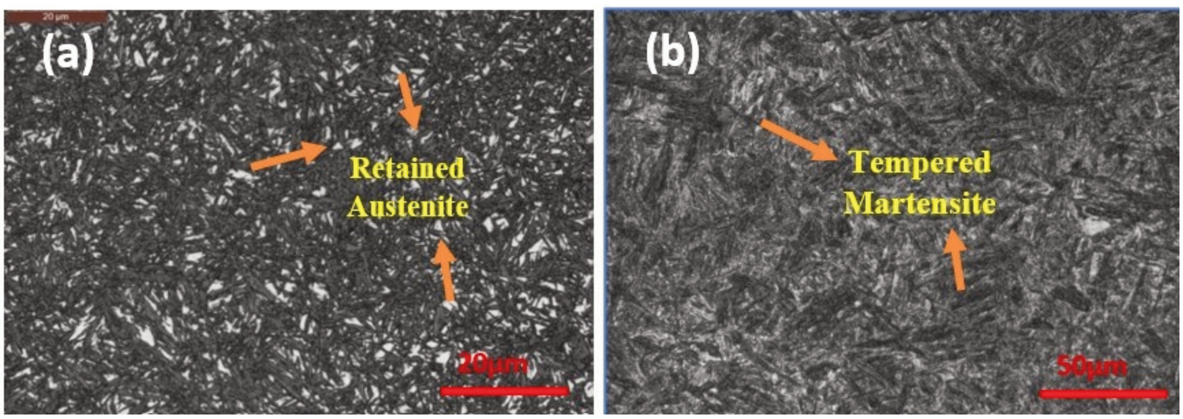

Figure 3. *Sample "A" (C+H+T) a) case micro structure at 1000X magnification; b) core micro structure at 500X magnification*

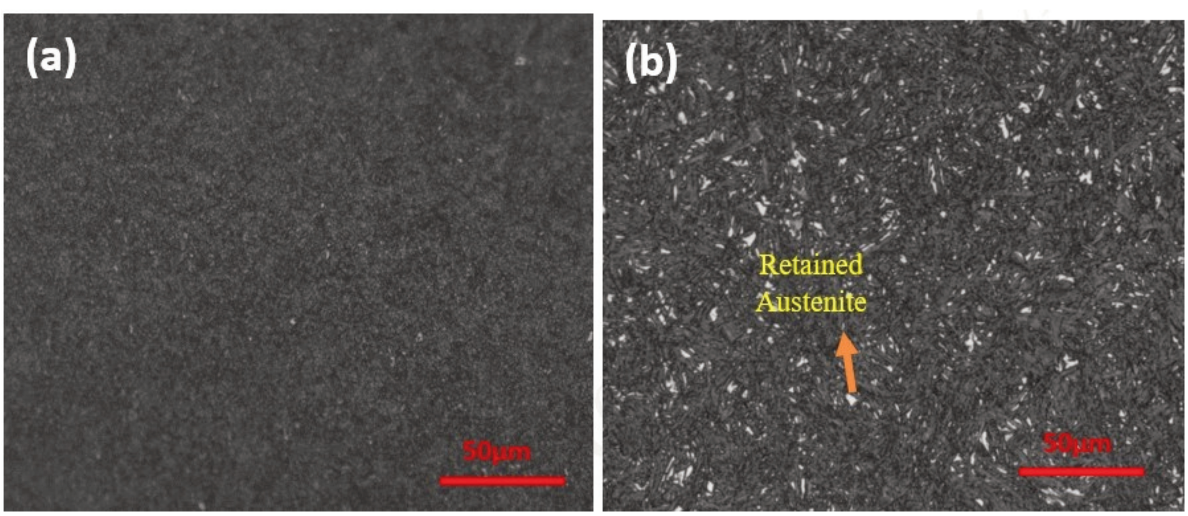

Figure 4. *a) EN36C; b) AISI 9315 case micro structure at 500X magnification (C+H+T+S+T)*

austenite is additionally influenced by carbon enrichment in the austenitic phase during carburizing and quenching processes. The observed increase in retained austenite with increasing Mo content in the present study is therefore attributed to the combined effects of reduced Ms temperature and enhanced carbon redistribution.

During tempering, fine Mo-rich carbide precipitates can form, contributing to precipitation strengthening and improved resistance to softening. This effect is particularly beneficial in maintaining hardness and wear resistance in carburized case-hardened steels.

A closer examination of the case microstructure in AISI 9315 unveiled a substantial 20% retained austenite content. This phase, recognized for its softer nature, elevated ductility, lower strength, and heightened toughness, plays a pivotal role in determining the material's properties [14]. However, the inherent instability of retained austenite under high-stress conditions necessitates its reduction to lower levels for an in-depth exploration of its tensile properties. Retained austenite presents an additional intriguing aspect in its resistance to fatigue crack growth. This is attributed to its softer nature and its proximity to the adjacent martensitic phase, characterized by high strength and superior mechanical properties. The quest, therefore, is to curtail retained austenite to minimal levels, while retaining the benefits it offers in terms of fatigue resistance, to ensure the optimization of the material's performance in demanding applications [16].

Sub-zero treatments were conducted to reduce retained austenite, as achieving a fully martensitic structure during hardening is challenging, leaving some retained austenite in hardened steel. Conventional metallographic techniques fail to detect retained austenite unless its concentration exceeds 20%. The presence of retained austenite significantly impairs mechanical properties, preventing the steel from attaining maximum hardness, even when cooled at rates exceeding the critical cooling rate. The amount of retained austenite is strongly influenced by the steel's chemical composition [15-16].

The microstructure of the steel samples after sub-zero treatment is shown in detail in Figure 4. The EN36C steel variety, in particular, showed a significant decrease in retained austenite. To stimulate the transformation of retained austenite within the unfinished product is the main goal of cold treatments, which are carried out at temperatures as low as -60 °C, -100 °F, or even lower. The dimensional stability that this change imparts is essential for later finishing processes [9]. In addition to providing dimensional stability and improved tool performance, these results emphasise the strategic use of cryogenic treatments to reduce retained austenite. They also emphasise the significance of exact treatment timing in order to minimize the risk of cracking [17-18].

Figures 5, 6, and 7 offer comprehensive insights into the microstructures of both the case and core regions of the steel samples, which have undergone sub-zero treatment. A notable reduction in the presence of retained austenite (RA) is observable in these microstructures compared to the samples before sub-zero treatment (Figure 8). The levels of RA were quantified using a standardized phase analysis method, and the detailed RA content for the various heat treatments is summarized in Table 2. It is worth highlighting the distinct responses of the AISI 9315 steel sample to different heat treatment regimens. When subjected to heat treatment and subsequent tempering, this sample exhibited no discernible RA. However, the same AISI 9315 sample, after undergoing a sequence of carburizing, hardening, and tempering, demonstrated a notable 20% RA content [19].

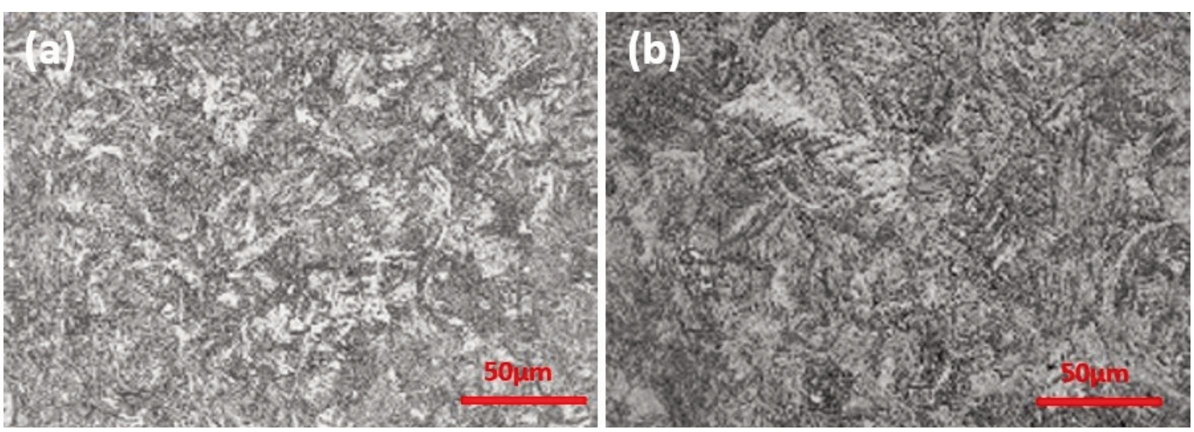

Figure 5. *Core micro structure of AISI 9315 samples at 500X magnification*

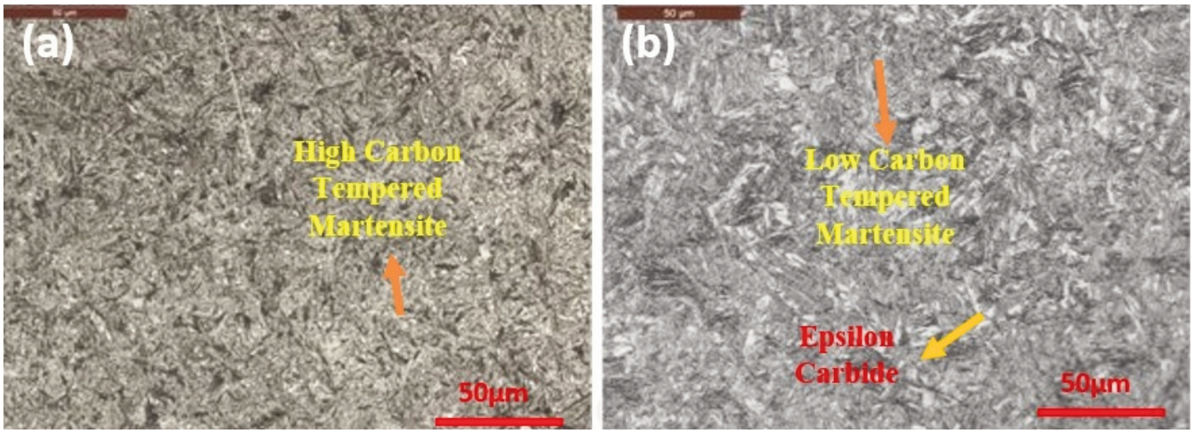

Figure 6. *EN36C: (a) HCTM with 5% RA; (b) Core: LCTM with Epsilon carbide*

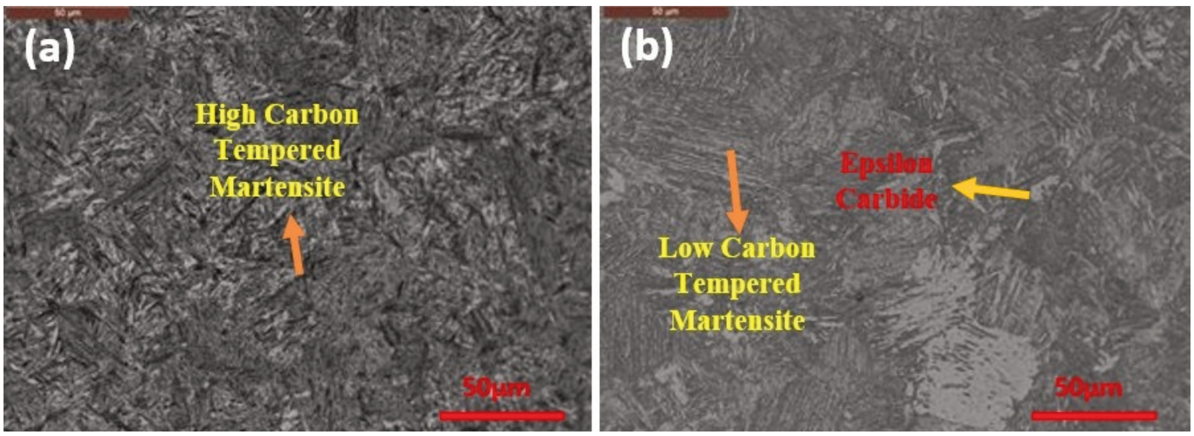

Figure 7. *AISI 9315 sub-zero treated: (a) Case HCTM with <5% RA; core: (b) LCTM with Epsilon carbide*

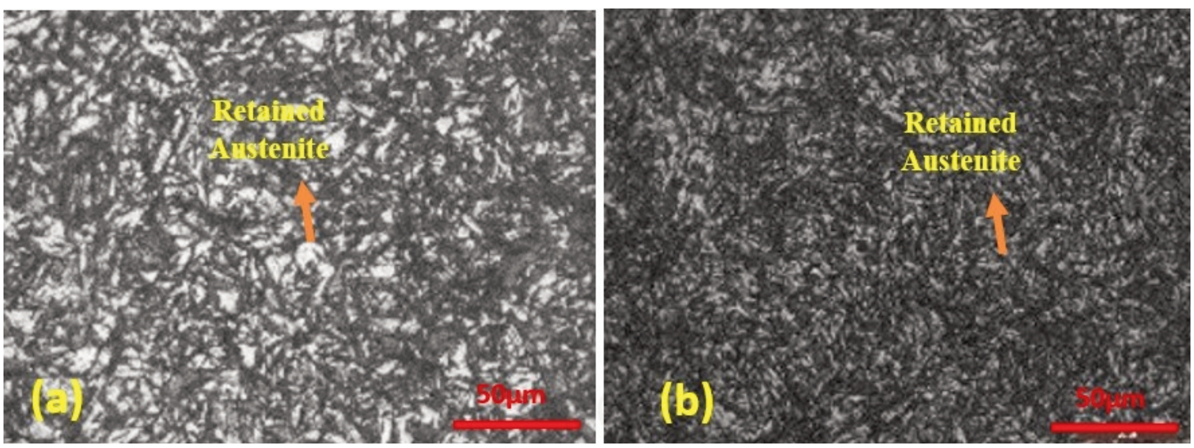

Figure 8. *Samples before sub-zero treatment: a) AISI 9315, b) EN36C*

Notably, with the introduction of sub-zero treatment to the carburized steel sample, the levels of retained austenite decreased to 10%. Furthermore, a subsequent tempering treatment following sub-zero treatment led to a further reduction, with RA levels declining to 8%. In contrast, the EN36C steel sample displayed RA levels tending towards the lower end of the spectrum, indicating the significant influence of molybdenum (Mo) on hardenability. The outcomes recorded in Table 2 unambiguously illustrate the pivotal role played by Mo content in shaping the microstructure and properties of the analyzed samples. These findings illuminate the intricate relationship between heat treatment, alloy composition, and the levels of retained austenite, with the results underscoring the influence of Mo content in modulating the microstructural features and mechanical properties of the investigated steel variants.

Table 2. *Percentage of RA in both steels at different stages of heat treatment*

	H+T	C+H+T	C+H+T+S	C+H+T+S+T
AISI 9315	0	~20	~10	~8
EN36C	0	~10	~5	~5

4. Mechanical Characterization

Tensile testing on heat-treated steel samples provided stress-strain graphs, correlating mechanical properties with microstructural characteristics for detailed analysis. The testing was carried out following the ASTM E8 standard, with dimensions measured as sub-sizes of the actual sample: Gauge length (G): Ø25.0 ± 0.1 mm; Width (B): Ø 6.0 ± 0.1 mm; Radius of fillet (R): 6 mm; Overall length (L): 100 mm.

The mechanical testing results for various heat-treated steel samples, detailed in Tables 3 and 4, show significant variations in Ultimate Tensile Strength (UTS) and Yield Strength (YS), as illustrated in Figures 9 and 10. Retained austenite (RA) negatively impacts these properties, with higher values observed in samples lacking RA.

Table 3. *Yield Strength (N/mm^2 or MPa)*

Sample	H+T		C+H+T	C+H+T+S +T
AISI 9315	1.303.960	1.084.655	626.866	497.512
EN36C	1.119.395	1.068.182	1.043.671	936.429

Table 4. *Ultimate Tensile Strength (N/mm^2 or MPa)*

Sample	H+T		C+H+T	C+H+T+S+ T
AISI 9315	1.398.773	1.387.799	946.379	615.810
EN36C	1.387.779	1.389.519	1.071.310	949.696

The study reveals that retained austenite levels and molybdenum (Mo) concentration significantly influence the steel's mechanical properties, highlighting the complex relationship between microstructure and tensile performance variations in the steel. The unambiguous evidence of the substantial influence of molybdenum content on tensile properties highlights the complex interactions among microstructure, material performance, and alloy composition [15, 20].

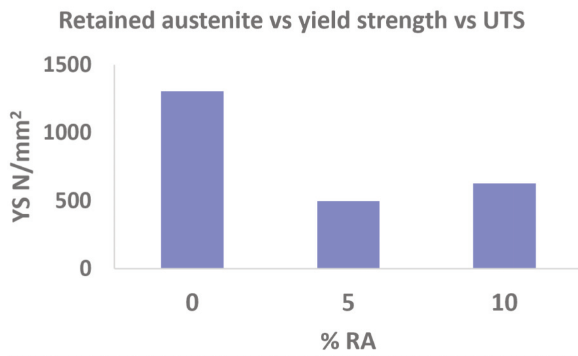

Figure 9. *Variation of AISI 9315 steel sample RA levels vs yield strength and UTS*

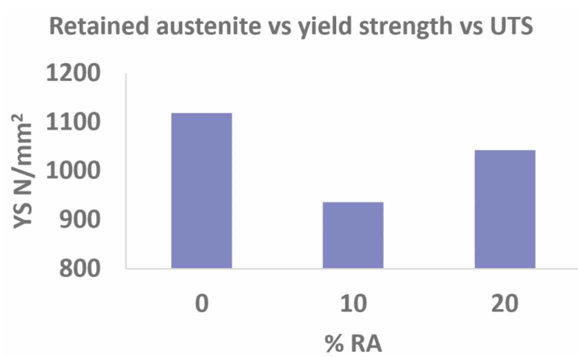

Figure 10. *Variation of EN36C steel sample RA levels vs yield strength and UTS*

4.1. Measurement of Case Depth

Finding the case depth, which is frequently defined as the depth below the surface at which a given property threshold is reached, is an important parameter in the characterization of materials [14]. Examples of exemplary parameters for an effective case depth are case depth to a carbon content of 0.4 wt% or to a hardness of 50 HRC [14]. Although the term "total case depth" is also used, it is widely regarded as being too ambiguous to be employed as a comprehensive specification because most carburized components exhibit a smooth transition between case and core features [14]. ASTM B934-10 was used for studying the case depth.

Figure 11 depicts the effective case depth of AISI 9315 and EN36C. Effective case depth, as measured to a specified hardness threshold, is quantified using a microhardness traverse on a polished metallographic section cut perpendicular to the surface. Vickers hardness, with a standard load of 0.5 kgf, is employed to obtain VHN values, which are subsequently converted to HRC values. To determine the Effective Case Depth (ECD), the ASTM standard was adhered to, considering the case drop (50 HRC = 513 HV = 542 HK). In cases where surface hardness is a significant specification, it can be derived by extrapolating subsurface microhardness values to the surface. Alternatively, surface hardness can be defined as the microhardness value at a depth of 0.1 mm (0.004 in.) beneath the material's surface. Precise microhardness readings closer than 0.1 mm (0.004 in.) to the edge of a polished section are challenging to obtain due to the occurrence of edge rounding during the polishing process. These methodologies and considerations are crucial for evaluating case depth and surface hardness, essential factors in assessing the quality and performance of carburized components.

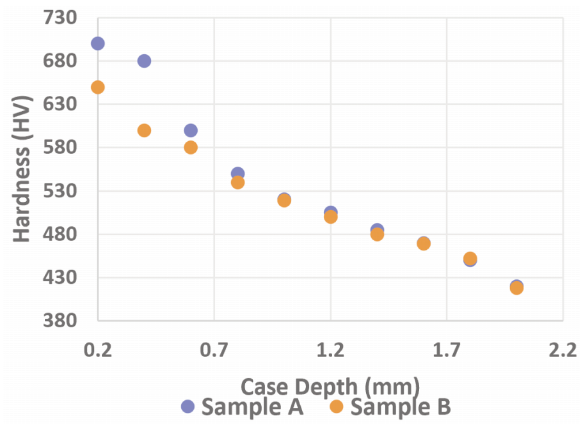

Figure 11. *Effective case depth profiles of AISI9315 (Sample A) and EN36C (Sample B)*

The examination of Figure 12 provides a lucid depiction of the comparative hardness levels exhibited by the heat-treated and tempered alloys in contrast to their carburized counterparts. In this visual representation, 'A' designates the AISI 9315 sample, while 'B' signifies the EN 36 C sample. The results unveiled in this context distinctly illustrate that the EN 36 C alloy, boasting a higher Mo content, manifests a notably greater hardness subsequent to heat treatment in comparison to the AISI 9315 counterpart. This differentiation in hardness profiles can be attributed to the distinct alloy compositions of these two materials, with molybdenum content emerging as a decisive factor influencing their heat treatment response [21-23]. It is noteworthy that the alteration in hardness levels observed between these alloys is instrumental in understanding the diverse mechanical characteristics and performance attributes exhibited by the materials, and this intricacy underscores the significant role played by alloy composition, particularly the presence of molybdenum, in shaping their heat treatment outcomes.

4.2. Fractography Studies

The detailed examination of fracture surfaces was carried out using a SEM Tescan Vega III instrument, offering invaluable insights into the intricate mechanisms underlying ductile fracture. Notably, the fractography studies were exclusively conducted on the concluding set of samples that had undergone sub-zero treatment, providing a specific focus on this critical aspect of the investigation. The fractography analysis facilitated the identification of crucial

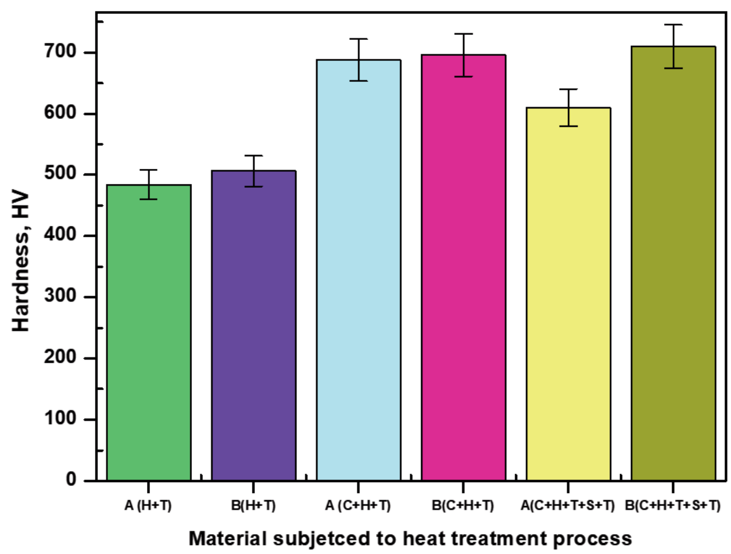

Figure 12. *Hardness plot with y-error for all the materials subjected to heat treatment process*

phenomena including the initiation, growth, and eventual coalescence of microvoids, shedding light on their precise mechanisms [21-23]. Additionally, this analysis revealed compelling correlations between the size and shape of these voids, often referred to as dimples, and various influential factors such as stress state and material cleanliness. The illuminating fractography results, as illustrated in Figures 13 and 14, encapsulate the visual evidence of the identified fracture mechanisms and provide a tangible link between the microstructural features and the materials' response to mechanical stress. This fractographic analysis serves as a vital component of the broader study, contributing essential insights into the fracture behaviour and performance characteristics of the investigated steel samples subjected to sub-zero treatment.

The analysis of Figures 13 (b) and 14 (b) reveals a conspicuous and noteworthy influence exerted by the varying molybdenum (Mo) content in the Ni-Cr-Mo steels on their failure behavior [24-25]. The fractography investigations conducted on both samples illuminate the ductile fracture mechanisms, evidenced by the presence of characteristic dimples within the microstructures [26-28]. A particularly intriguing observation arises from the data – an increase in Mo content correlates with a discernible reduction in the occurrence of flaking behavior [29-31]. This intriguing relationship underscores the significance of molybdenum in shaping the failure characteristics of the materials. This nuanced behavior observed in the fractography findings can be attributed, at least in part, to the percentage of retained austenite (RA) within the samples [32-35].

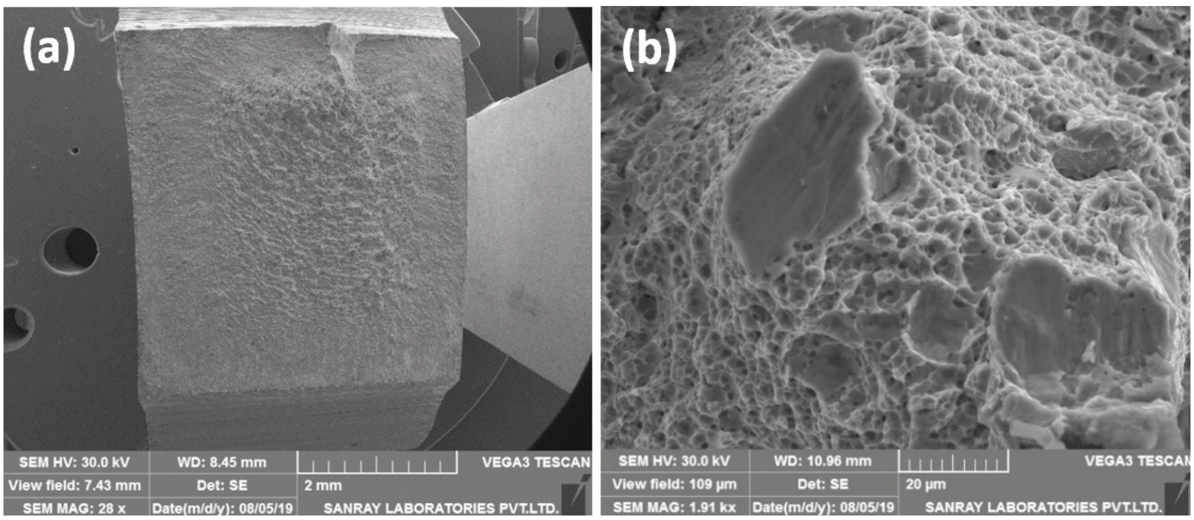

Figure 13. *Fractography of the tensile test specimens of AISI 9315 steel obtained at a) 470X (b) 1.9kX*

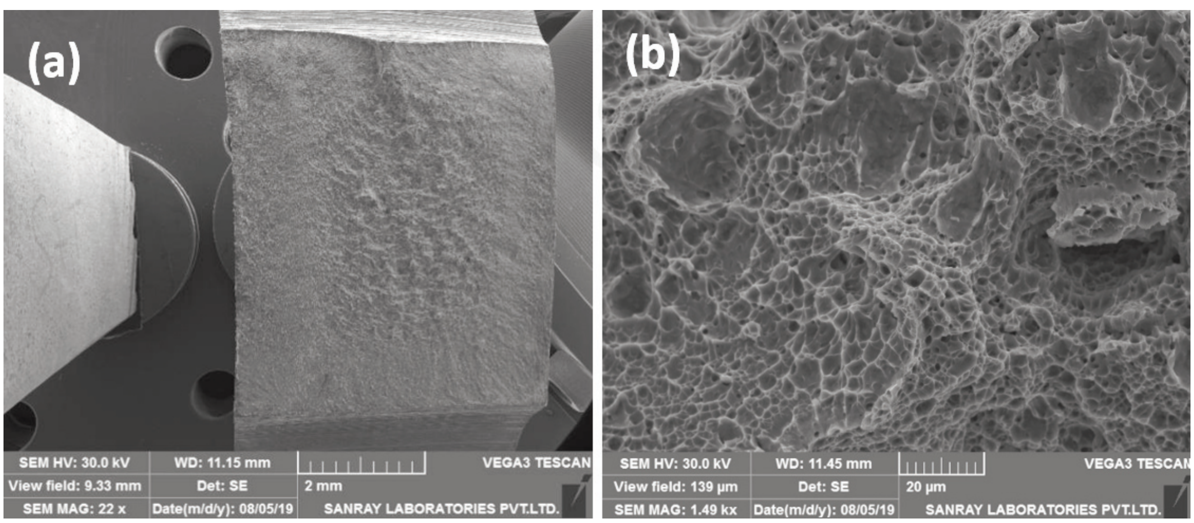

Figure 14. *Fractography of the tensile test specimens of EN36C obtained at a) 20X; b) 1.5kX*

Specifically, the AISI9315 steel exhibited a higher RA content of 8%, in contrast to the EN36C steel's lower 5% RA content, which corresponds to its elevated Mo content in the post-sub-zero treated sample. It is evident that the presence of retained austenite introduces a degree of softness within the microstructure, as vividly demonstrated in Figure 13 (b). In this context, molybdenum emerges as a pivotal actor, playing a substantial role in reducing the levels of retained austenite, as underscored by the results of the sub-zero treatment experiments [26]. These findings serve as a resounding testament to the profound impact of even slight variations in Mo content on the material's fracture behavior and properties, which, in critical cases, could lead to product rejection in industrial applications. Consequently, these insights underscore the paramount importance of carefully considering both chemical composition and processing methods in the realm of metallurgy, as they wield substantial influence over the ultimate properties of metallurgical products [36-37].

5. Conclusion

In conclusion, this study has elucidated the intricate interplay between alloy composition, particularly molybdenum (Mo) content, heat-treatment conditions, microstructural evolution, and mechanical properties of Ni-Cr-Mo case-hardening steels, namely AISI 9315 and EN36C. The investigation provided several important insights into the behavior of carburized steels under industrial heat-treatment conditions.

* **Influence of Molybdenum:** The study clearly demonstrated the significant role of molybdenum in improving the hardenability and mechanical performance of the investigated steels. AISI 9315 steel, containing relatively higher Mo content, exhibited improved case hardness, tensile strength, and impact resistance compared to EN36C steel. The hardness values in the carburized case region reached approximately 700–750 HV, while the tensile strength showed an improvement of nearly 8–12% in the higher-Mo steel under similar processing conditions.

* **Retained Austenite Dynamics:** Retained austenite (RA) was identified as a critical microstructural constituent influencing hardness and strength. The retained austenite content was observed to vary within the range of approximately 8–20% depending on steel composition and post-treatment conditions. Higher RA levels were associated with comparatively lower hardness and tensile strength due to increased phase stability. Sub-zero treatment effectively reduced RA content and enhanced martensitic transformation, leading to measurable improvements in hardness and dimensional stability. The role of Mo in influencing martensite transformation behavior and RA stability was clearly evident.

* **Microstructural and Fractography Observations:** Microstructural characterization confirmed the formation of a hard martensitic carburized case with a comparatively tougher core structure. Fractography analysis revealed predominantly ductile fracture features with localized brittle/flaky regions in higher-Mo steels, indicating the influence of alloy chemistry and retained austenite on fracture behavior. The observed fracture morphology correlated well with the tensile and impact properties obtained after heat treatment.

* **Industrial Relevance:** The findings are highly relevant for industrial applications involving gears, shafts, mining tools, and heavy-duty transmission components, where carburized steels require an optimum balance between surface hardness, wear resistance, fatigue strength, and core toughness. The achieved effective case depth of approximately 0.8–1.2 mm and improved mechanical response demonstrate the suitability of higher-Mo Ni-Cr-Mo steels for demanding service conditions.

* **Metallurgical Implications:** The study emphasizes that even minor variations in molybdenum content within similar alloy systems can substantially alter transformation behavior, retained austenite stability, hardness distribution, and fracture response after carburizing and heat treatment. The results highlight the necessity of carefully controlling alloy chemistry and processing parameters to optimize the performance of case-hardened steels.

Overall, the present work provides useful metallurgical insights into the role of molybdenum in carburized Ni-Cr-Mo steels and offers practical guidance for alloy selection, heat-treatment optimization, and performance enhancement of critical engineering components used in automotive, mining, aerospace, and heavy engineering industries.

Supplementary Material
S1: Tensile Test

Tensile testing was performed to evaluate the mechanical properties of the investigated Ni-Cr-Mo steels subjected to different heat-treatment conditions. The tests were conducted using a 60-ton universal testing machine (UTM) (Figure S1) in accordance with ASTM E8/E8M standards. During testing, the specimen was gripped at both ends and subjected to a uniaxial tensile load at a constant crosshead speed until fracture.

The applied load and corresponding displacement were continuously recorded and converted into engineering stress–strain curves. The mechanical properties obtained from the tensile tests included yield strength (YS), ultimate tensile strength (UTS), percentage elongation, and reduction in area.

The ultimate tensile strength (UTS) was determined as:

Maximum load divide by the original cross-sectional length area of the tensile.

The percentage elongation after fracture was calculated using:

Elongation = $(L_f - L_0)/ L_0 \times 100$

Where,

L_f - final gauge length

L_o - original gauge length

The percentage reduction in area was determined using:

Reduction in area = $(A_0 – A_f)/A_0 \times 100$

Where,

A_0 - original cross-sectional area

A_f - final cross-sectional area.

Figure S1. *Universal testing machine used for tensile testing. ASI UTM Machine 60 Tonnes*

S2. Tensile Specimen Preparation

Tensile specimens were prepared according to the ASTM E8/E8M sub-size specimen geometry due to the limited dimensions of the heat-treated samples. The dimensions of the tensile specimens are illustrated in Figure S2.

The principal dimensions were as follows:

Parameter	Description	Dimension (mm)
G	Gauge length	25.0 ± 0.1
W	Gauge width	6.0 ± 0.1
T	Thickness	As machined
R	Fillet radius	6.0
L	Overall length	100
A	Length of reduced section	32
C	Grip length	30
D	Grip width	10

S3. Tensile Properties of Heat-Treated Ni-Cr-Mo Steels

Tensile testing was carried out on Type A and Type B Ni-Cr-Mo steels subjected to various heat-treatment conditions, including hardening and tempering (H+T), carburizing followed by hardening and tempering (C+H+T), and carburizing followed by hardening, sub-zero treatment, and tempering (C+H+T+S+T). The resulting stress–strain curves were used to evaluate the influence of heat treatment on mechanical performance and to establish correlations with the observed microstructures.

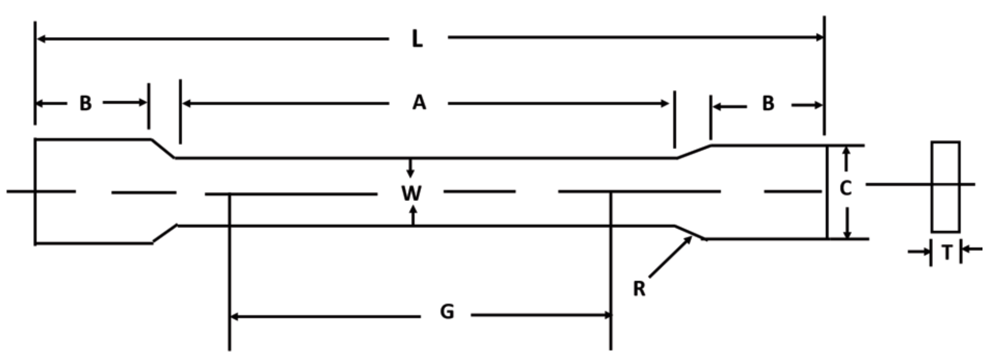

Figure S2. *ASTM E8 tensile sample preparation (sub size method)*

Comparative analysis of Mechanical Properties of *Type A and B* Ni-Cr-Mo Steels

A. Yield Strength (N/mm^2 or MPa)

Sample	H+T		C+H+T	C+H+T+S+T
Type A	1.303.960	1.084.655	626.866	497.512
Type B	1.119.395	1.068.182	1.043.671	936.429

B. Ultimate Tensile Strength (N/mm^2 or MPa)

Sample	H+T		C+H+T	C+H+T+S+T
Type A	1.398.773	1.387.799	946.379	615.810
Type B	1.387.779	1.389.519	1.071.310	949.696

S3.3 Stress–Strain Curves

The engineering stress–strain curves corresponding to the various heat-treatment conditions are presented in Figures S3–S8.

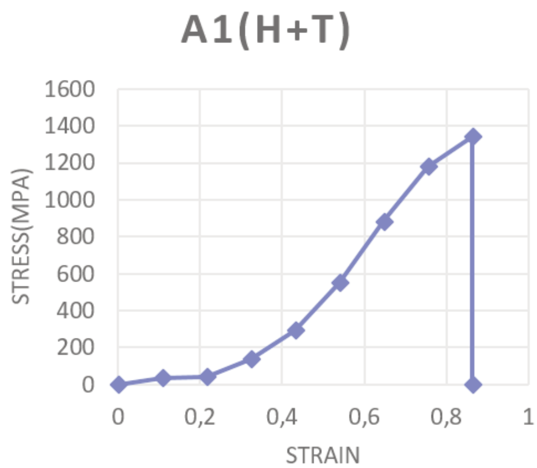

Figure S5. *Engineering stress–strain curve of Type B steel subjected to hardening and tempering*

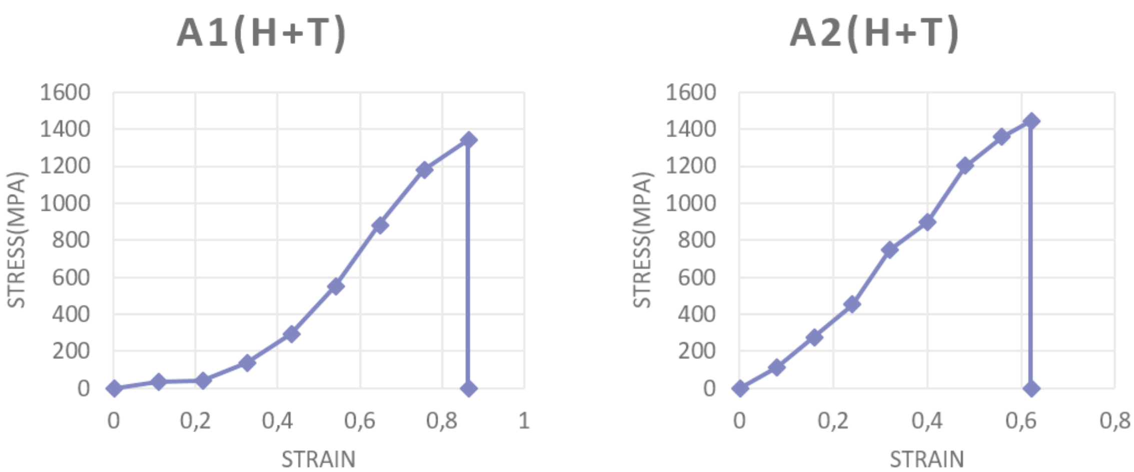

Figure S3. *Engineering stress–strain curve of Type A steel subjected to hardening and tempering*

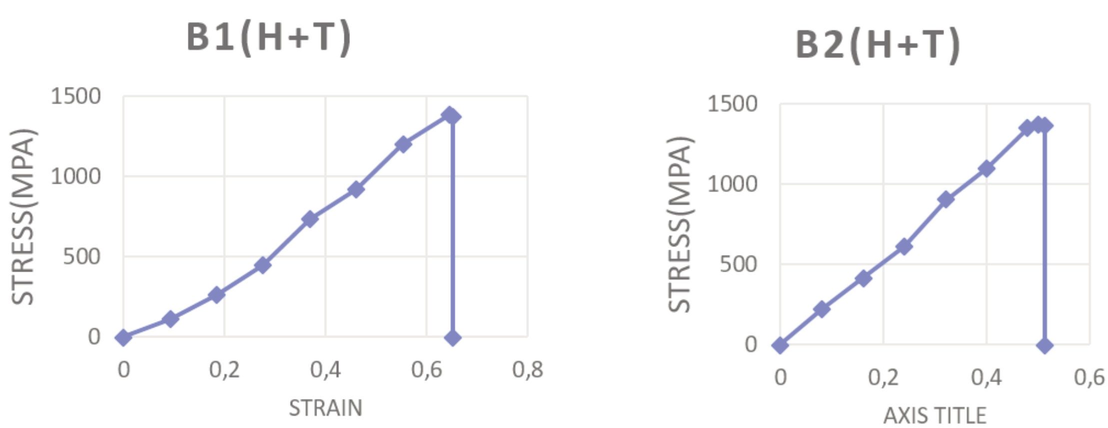

Figure S4. *Engineering stress–strain curve of Type B steel subjected to hardening and tempering*

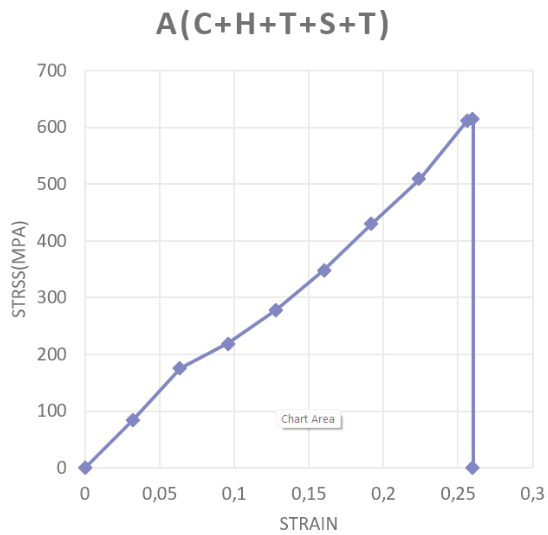

Figure S6. *Engineering stress–strain curve of Type A steel subjected to carburizing, hardening, sub-zero treatment, and tempering*

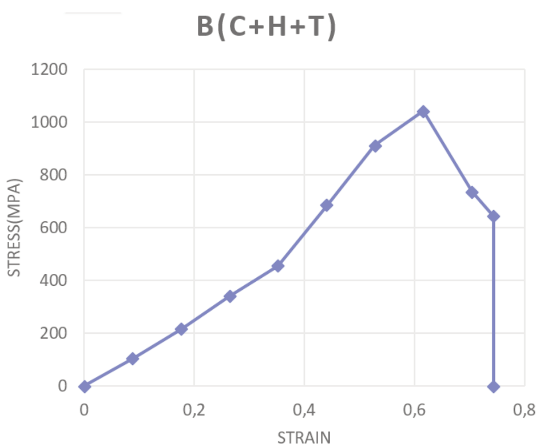

Figure S7. *Engineering stress–strain curve of Type B steel subjected to carburizing, hardening, and tempering*

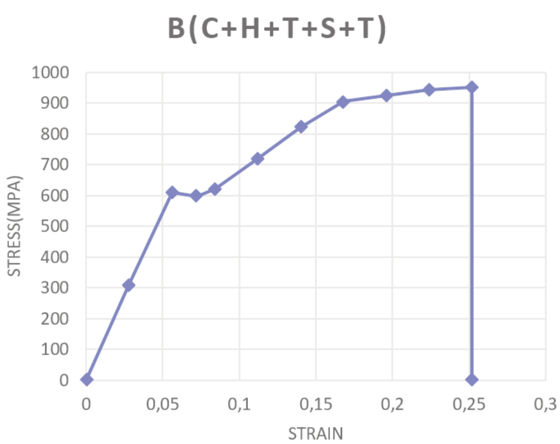

Figure S8. *Engineering stress–strain curve of Type B steel subjected to carburizing, hardening, sub-zero treatment, and tempering*

Acknowledgments

Authors thank Central Instrumentation Facility (CIF) at OP Jindal University for the SEM characterization. VKK thanks Metallurgy staff at OPJU for their support in preparation of the samples. Authors MKP and VKK express thanks to the Management of OP Jindal University for their support and encouragement for conducting this research work.

Author Contributions

Conceptualization, K.V.K. and M.K.P.; methodology, M.K.P.; validation, K.V.K. and M.K.P.; formal analysis, K.V.K., and M.K.P.; investigation, K.V.K. and M.K.P.; resources, K.V.K. A.M. and M.K.P; data curation, K.V.K.; writing—original draft preparation, K.V.K.; writing—review and editing, M.K.P.; visualization, K.V.K. and MKP; supervision, M.K.P.; project administration, M.K.P.; Funding acquisition; M.K., A.M.

Author ORCiD

Varun Kumar Kurapati (0000-0002-4110-5832), Makkuva Kalyan Phani (0000-0002-9764-5117), Arghya Majumder (0000-0001-8677-7838).

Data Availability

The datasets used and/or analyzed during the current study available from the corresponding author on reasonable request.

Conflicts of Interest

The authors declare there are no conflicts of interest.

References

[1] V. Mishra, K. Chakraborty, Machinability of nickel chromium case hardened steel (EN36C), Global Journal of Researches in Engineering: A Mechanical and Mechanics Engineering, 19(1) (2019) 27–34.

[2] P. S. Prevéy, J. T. Cammett, The effect of shot peening coverage on residual stress, cold work and fatigue in a Ni–Cr–Mo low alloy steel, Proceedings of the International Conference on Shot Peening, 16–20 September 2002, Garmisch-Partenkirchen, Germany.

[3] S.-G. Park, K.-H. Lee, K.-D. Min, M.-C. Kim, B.-S. Lee, Characterization of phase fractions and misorientations on tempered bainitic/martensitic Ni–Cr–Mo low alloy RPV steel with various Ni content, Materials Science Forum, 783–786 (2014) 2656–2661. https://doi.org/10.4028/www.scientific.net/MSF.783-786.2656

[4] R.U. Khan, Vacuum gas carburizing—fate of hydrocarbons, Doctoral Dissertation, Karlsruhe Institute of Technology (KIT), Karlsruhe, Germany, 2008.

[5] H.K.D.H. Bhadeshia, Developments in martensitic and bainitic steels: role of the shape deformation, Materials Science and Engineering A, 378(1–2) (2004) 34–39. https://doi.org/10.1016/j.msea.2003.10.328

[6] A. Majumder, M.K. Phani, Green steel technology: a viable approach for sustainable world, in Proceedings of the International Conference on Metallurgical Engineering and Centenary Celebration, Springer Nature, Singapore, 2023, pp. 366–374. https://doi.org/10.1007/978-981-99-6904-8_31

[7] G.F. Vander Voort, Etching techniques for image analysis, Microstructural Science, 9 (1981) 137–154.

[8] ASTM International, ASTM B934-10: Standard test method for effective case depth measurement of ferrous metals, ASTM International, West Conshohocken, PA, USA, 2010.

[9] N. Bharat, V. Mishra, K. Chakraborty, Machining behavior of EN24 and EN36C steels, International Journal of Innovative Engineering and Technology, 12(4) (2019) 1–6.

[10] Linde AG, Sub-zero treatment of steels, Linde AG, Munich, Germany. 2021

[11] C.-S. Oh, J.-H. Song, Crack growth and closure behaviour of surface cracks under pure bending loading, International Journal of Fatigue, 23(3) (2001) 251–258.

https://doi.org/10.1016/S0142-1123(00)00086-0

[12] F. Hairer, A. Karelová, C. Krempaszky, E. Werner, T. Hebesberger, Etching techniques for microstructural characterization of complex phase steels by light microscope, Technical Report, Christian Doppler Laboratory of Material Mechanics of High-Performance Alloys, Chair of Materials Science and Mechanics of Materials, Technical University of Munich, Munich, Germany, 2022.

[13] K. Palaniradja, N. Alagumurthi, V. Soundararajan, Residual stresses in case hardened materials, The Open Materials Science Journal, 4 (2010) 92–102. https://doi.org/10.2174/1874088X01004010092

[14] R.A. Cutler, W.C. Leslie, Effects of temperature on the fracture toughness of carburizing steels for high-temperature applications, Journal of Testing and Evaluation, 11(1) (1983) 3–15. https://doi.org/10.1520/JTE10709J

[15] C.J. Schroeder, Metallurgical failure analysis: Case study of a fractured hitch, Case Studies in Engineering Failure Analysis, 4 (2015) 54–60. https://doi.org/10.1016/j.csefa.2015.07.001

[16] A.M. Borisov, A.M. Shkatova, S.B. Vikhriev, Structure and properties of Ni–Cr–Mo–V rotor steels, Metal Science and Heat Treatment, 31(11–12) (1989) 848–852. https://doi.org/10.1007/BF00733664

[17] V. Mishra, N. Bharat, K. Chakraborty, Comparative assessment on the machinability of EN24 and EN36C steels, International Journal of Engineering and Advanced Technology, 8(3) (2019) 1136–1140.

[18] S.S. Gill, R. Singh, J. Singh, H. Singh, Metallurgical principles of cryogenically treated tool steels—A Review on the current state of science, The International Journal of Advanced Manufacturing Technology, 54(1–4) (2011) 59–82. https://doi.org/10.1007/s00170-010-2905-9

[19] P. Jurči, I. Dlouhý, P. Priknerová, Z. Mrštný, Effect of sub-zero treatment temperatures on hardness, flexural strength, and fracture toughness of vanadis 6 ledeburitic die steel, Metals, 8(12) (2018) 1047. https://doi.org/10.3390/met8121047

[20] T.M. Pugacheva, A.V. Klimenko, A.P. Amosov, Steel analysis for rock bits up to 150.0 mm diameter, CIS Iron and Steel Review, 17(3) (2009) 123–131.

[21] K.V. Kumar, M.K. Phani, Microstructural and mechanical characterization of parallel layered WC–NiCr weld overlay on 080M40 steel substrate prepared using additive manufacturing, Materials Today: Proceedings, 67 (2022) 501–506. https://doi.org/10.1016/j.matpr.2022.02.422

[22] D. Rai, B. Singh, J. Singh, Characterisation of wear behaviour of different microstructures in Ni–Cr–Mo–V steel, Wear, 263(1–6) (2007) 821–829. https://doi.org/10.1016/j.wear.2006.12.014

[23] H.K.D.H. Bhadeshia, Steels for bearings, Progress in Materials Science, 57(2) (2012) 268–435. https://doi.org/10.1016/j.pmatsci.2011.06.002

[24] G.E. Totten, L.C.F. Canale, R.A. Mesquita, Failure analysis of heat treated steel components, ASM International, Materials Park, OH, USA, 2008.

[25] M. Bepari, K. Shorowordi, Effects of molybdenum and nickel additions on the structure and properties of carburized and hardened low carbon steels, Journal of Materials Processing Technology, 155–156 (2004) 1972–1979. https://doi.org/10.1016/j.jmatprotec.2004.04.060

[26] M.K. Phani, Role of indentation size effect in micro-indentation testing on different materials, International Journal of Creative Research Thoughts, 11(3) (2023) i178–i186.

[27] M.K. Phani, R.D. Patidar, S.S. Chakrabarti (Eds.), Preface: Proceedings of the 5th International Conference on Advances in Steel, Power and Construction Technology (ICASPCT 2022), AIP Conference Proceedings, 2888(1) (2023) 010001. https://doi.org/10.1063/12.0018170

[28] M.K. Phani, S. Kanhed, S. Chakrabarti, R.D. Patidar, Editorial Preface on the Proceedings of the 5th International Conference on Advances in Steel, Power and Construction Technology (ICASPCT 2022), Materials Today: Proceedings, 67 (2022) 550–551. https://doi.org/10.1016/j.matpr.2022.05.391

[29] G. Khalaj, M.J. Khalaj, Modeling layer thickness of duplex ceramic (chromium carbonitride) coating on cold work tool steel using fuzzy logic, Journal of Intelligent & Fuzzy Systems, 26(5) (2014) 2229–2237. https://doi.org/10.3233/IFS-130896

[30] S. Yan, M. Taheri, B. Ahadi, K. Shirvani, G. Khalaj, M. Šlapáková, M. Jafarzadegan, A new method of applying CrNbTaMoTi high entropy coating using the laser cladding/laser remelting technique, Materials Chemistry and Physics, 333 (2025) 130339. https://doi.org/10.1016/j.matchemphys.2024.130339

[31] A. Heydarian, A. Najafi, G. Khalaj, Enhancement of low-zinc phosphate coatings with addition of Ni^{2+} and Mn^{2+} cations: structure, corrosion resistance and paint adhesion, Journal of Materials Research and Technology, 30 (2024) 7308–7327. https://doi.org/10.1016/j.jmrt.2024.05.103

[32] G. Khalaj, M.J. Khalaj, Application of ANFIS for modeling of layer thickness of chromium carbonitride

coating, Neural Computing and Applications, 25(3–4) (2014) 685–694. https://doi.org/10.1007/s00521-012-1290-x

[33] G. Khalaj, M.J. Khalaj, Modeling layer thickness of duplex ceramic coating on tool steel using fuzzy logic and artificial neural networks, Neural Computing and Applications, 24(7–8) (2014) 1683–1692. https://doi.org/10.1007/s00521-012-0994-2

[34] G. Khalaj, H. Pouraliakbar, Computer-aided modeling for predicting layer thickness of a duplex treated ceramic coating on tool steels, Ceramics International, 40(4) (2014) 5515–5522. https://doi.org/10.1016/j.ceramint.2013.10.141

[35] X. Yan, J. Hu, X. Zhang, W. Xu, Obtaining superior low-temperature wear resistance in Q&P-Processed medium Mn steel with a low initial hardness, Tribology International, 175 (2022) 107803. https://doi.org/10.1016/j.triboint.2022.107803

[36] C. Shen, C. Wang, X. Wei, Y. Li, S. van der Zwaag, W. Xu, Physical metallurgy-guided machine learning and artificial intelligent design of ultrahigh-strength stainless steel, Acta Materialia, 179 (2019) 201–214. https://doi.org/10.1016/j.actamat.2019.08.033

[37] Y. Li, D. San Martín, J. Wang, C. Wang, W. Xu, A review of the thermal stability of metastable austenite in steels: martensite formation, Journal of Materials Science & Technology, 91 (2021) 200–214. https://doi.org/10.1016/j.jmst.2021.03.020

ULOGA MOLIBDENA U Ni-Cr-Mo ČELICIMA NAMENJENIM ZA PRIMENU U RUDARSTVU – INDUSTRIJSKA PERSPEKTIVA

Varun Kumar Kurapati [a], Makkuva Kalyan Phani [a, *], Arghya Majumder [b]

[a] Katedra za metalurško inženjerstvo, O.P. Jindal Univerzitet, Rajgarh, Čatisgar, Indija
[b] Fakultet za rudarstvo i metalurgiju, Univerzitet Kazi Nazrul, Asansol, Zapadni Bengal, Indija

Apstrakt

Čelici legirani niklom, hromom i molibdenom (Ni-Cr-Mo) imaju široku primenu u zahtevnim inženjerskim primenama koje zahtevaju visoku čvrstoću, otpornost na habanje i otpornost na zamor materijala. U ovom radu ispitan je uticaj sadržaja molibdena na razvoj mikrostrukture i mehanička svojstva cementiranih čelika EN36C i AISI 9315. Čelici su podvrgnuti gasnoj cementaciji na temperaturi od 920 °C u komornoj peći za kaljenje sa zaštitnom atmosferom, nakon čega su usledili kaljenje i otpuštanje. Detaljna karakterizacija obuhvatila je analizu mikrostrukture, merenje tvrdoće, određivanje dubine cementiranog sloja, ispitivanje zateznih svojstava, ispitivanje udarne žilavosti i fraktografsku analizu. Rezultati su pokazali značajne razlike u mikrostrukturi i mehaničkim svojstvima između ispitivanih vrsta čelika. Čelik AISI 9315, sa relativno većim sadržajem molibdena, pokazao je veću prokaljivost, veću tvrdoću, povoljnije karakteristike cementiranog sloja i bolja mehanička svojstva u poređenju sa čelikom EN36C. Takođe su uočene razlike u sadržaju zaostalog austenita i mehanizmima loma u zavisnosti od sadržaja molibdena i odgovora materijala na termičku obradu. Rezultati istraživanja potvrđuju značajnu ulogu molibdena u kontroli faznih transformacija i unapređenju ukupnih svojstava cementiranih Ni-Cr-Mo čelika namenjenih za primenu u rudarstvu.

Ključne reči: *Ni-Cr-Mo čelici; Gasna cementacija; Dubina cementiranog sloja; Mikrotvrdoća; Fraktografija*